RSC Advances

PAPER

View Article Online
View Journal | View Issue

Cite this: *RSC Adv.*, 2026, **16**, 23443

Heteroatom-doped reduced graphene oxide electrochemical sensor for sensitive dopamine detection with preliminary clinical evaluation of neurotransmitter dysregulation in pediatric epilepsy

Fatma Besbes, [ab] Zouhour Hsine,[b] Said Galai, *[cd] Ichraf Kraoua, [ce] Rym Mlika [b] and Hafsa Korri-Youssoufi *[a]

Monitoring dopamine (DA) levels in biological fluids is highly informative for the early diagnosis and therapeutic management of neurological disorders such as Parkinson's disease, schizophrenia, attention-deficit/hyperactivity disorder (ADHD), and epilepsy, which represents a major pediatric neurological condition with wide clinical heterogeneity. In this study, we report a preliminary clinical evaluation of an electrochemical sensor developed for DA detection in the blood of pediatric epilepsy patients. The sensing platform is based on screen-printed carbon electrodes (SPCEs) modified with nitrogen-doped reduced graphene oxide (N-RGO) and nitrogen/sulfur co-doped reduced graphene oxide (S/N-RGO) to enhance electrocatalytic performance. Heteroatom incorporation into RGO significantly improved electron transfer kinetics, electroactive surface area, and sensing activity. Using chronoamperometry (CA) and differential pulse voltammetry (DPV), the N-RGO sensor achieved low detection limits of 6.8 nM and 7.9 nM, respectively, in buffer, with excellent selectivity in the presence of common interferents such as ascorbic acid and uric acid. High recovery rates (~100%) were obtained in commercial plasma and fresh human serum samples, including those collected from pediatric epilepsy patients. Notably, DA plasma concentrations were found to be lower in this heterogeneous group of epileptic patients, reflecting neurotransmitter dysregulation associated with epilepsy subtype and antiepileptic treatment (valproate). This work presents a sensitive electrochemical sensor capable of detecting and monitoring DA in blood and highlights its potential as a minimally invasive point-of-care tool for pediatric epileptic patients. With further development, this device could also be applied to assess DA levels in other neurological disorders.

Received 18th December 2025
Accepted 26th March 2026

DOI: 10.1039/d5ra09797e

rsc.li/rsc-advances

1 Introduction

Humanity faces a major challenge from numerous diseases, some curable and others incurable. Depending on the timing of diagnosis, a therapeutic solution may or may not be possible. Early detection of disease biomarkers is therefore essential, and the development of innovative analytical technologies remains central to improving diagnostic pathways. Among emerging health concerns, neurological disorders represent life-threatening risks, frequently leading to chronic disability. Parkinson's disease (PD) is a rapidly progressing neurodegenerative disorder that significantly reduces life expectancy.[1] The prevalence of Alzheimer's disease (AD) is expected to triple by 2050, posing a critical threat to the aging population[2]. Neurological disorders affecting children, such as ADHD[3] and epilepsy, are also on the rise, underscoring the urgent need for sensitive diagnostic tools capable of quantifying neurotransmitters (NTs) to better understand disease pathophysiology and progression.

In epilepsy, dopaminergic synaptic function is intimately linked to DA. Its dysregulation plays a key role due to interactions with other major NTs, including γ-aminobutyric acid (GABA) and glutamate. Several antiepileptic drugs, such as valproic acid (VAL), modulate DA levels to enhance GABAergic

[a]*Université Paris-Saclay, UMR-CNRS, Institut de Chimie Moléculaire et des Matériaux d'Orsay (ICMMO, ECBB, Bât Henri Moisson, 17 Avenue des Sciences, 91400 Orsay, France. E-mail: hafsa.korri-youssoufi@universite-paris-saclay.fr; Tel: +33-169157440*

[b]*Laboratory of Interfaces and Advanced Materials, Faculty of Science of Monastir, University of Monastir, 5019 Monastir, Tunisia*

[c]*Research Laboratory of Neurological Diseases of the Child (LR18SP04), Department of Clinical Biology, National Institute Mongi Ben Hmida of Neurology at Tunis, La Rabta 1007 Tunis, Tunisia*

[d]*Faculty of Sciences of Tunis, Department of Biology, University Tunis El Manar, Campus Universitaire El Manar I, 2092 Tunis, Tunisia*

[e]*Faculty of Medicine of Tunis, Rue de la Faculté de Médécine, University Tunis El Manar, 1007 Tunis, Tunisia*

inhibition, suppress excitatory glutamatergic pathways, and protect against seizures.[4,5] Across neurological diseases, DA dysregulation contributes to neurotransmitter imbalance and overall central nervous system (CNS) dysfunction.[6] Beyond its neuronal role, DA is secreted by peripheral organs such as the adrenal glands, where it serves as a precursor for adrenaline and noradrenaline. Elevated DA levels in peripheral blood can induce cardiovascular impairment, including tachycardia, hypertension, and heart failure.[7] In healthy individuals, DA concentrations in peripheral fluids are typically low (0.03–0.2 μM);[8,9] however, DA is also used clinically as an intravenous resuscitation agent, requiring strict quality control to ensure safety and efficacy.[10] Thus, developing sensitive, rapid, and cost-effective methods for monitoring DA levels in biological fluids is critical to support early diagnosis, therapeutic monitoring, and patient care.

Conventional methods for DA detection, such as high-performance liquid chromatography (HPLC),[11] flow injection-chemiluminescence,[12] fluorescence spectrophotometry,[13] and capillary electrophoresis (CE)-chemiluminescence,[14] offer high sensitivity but are often limited by complex instrumentation, high operational costs, time-consuming procedures, and poor anti-interference capability.[15] These constraints restrict their practical application in routine clinical testing and point-of-care (POC) settings. In contrast, electrochemical sensing provides rapid response, high sensitivity, and real-time monitoring, making it highly suitable for clinical applications and minimally invasive DA detection in biological fluids.[16]

The choice of electrode material is critical, as it governs the selectivity, sensitivity, and reproducibility of electrochemical detection. Glassy carbon electrodes (GCEs) are widely used due to their conductivity, wide potential window, and chemical stability.[17] However, SPCEs provide additional advantages for clinical applications, including larger electroactive surface areas, improved signal-to-noise ratios, excellent reproducibility, and disposability.[18,19] To enhance electroanalytical performance, SPCEs were modified with nanomaterials, such as metals nanoparticles, resulting in improved sensitivity for DA detection.[20] Graphene-based nanomaterials have attracted significant interest for electrochemical DA sensing because of their high conductivity and large specific surface area.[21,22] Incorporating heteroatoms (*e.g.*, nitrogen, sulfur) further enhances electrocatalytic activity by generating charged sites, modulating spin density, and strengthening interactions with target analytes.[23–25] Nitrogen[26,27] or sulfur[28] doping improves electron transfer and conductivity, whereas nitrogen/sulfur co-doping provides synergistic enhancements in electrocatalytic performance through spin and charge redistribution.[29] Heteroatom-doped RGO materials have been widely studied for sensing applications, including the detection of hazardous metals such as europium,[30] toxic pollutants,[31] catechol and hydroquinone.[32]

Several recent studies have explored heteroatom-doped graphene materials for electrochemical DA detection. Zhang and Liu[33] reported N-RGO electrodes for simultaneous detection of DA, ascorbic acid, and uric acid in buffer. The enhanced electrochemical response was attributed to strong π–π interactions between the graphene basal plane and the aromatic structure of the analytes, together with hydrogen bonding between pyridinic and pyrrolic nitrogen functionalities and the amine or hydroxyl groups of DA. Various recent work associated doped graphene with others nanomaterials to enhance the sensitivity, for example Zhong and *et al.*[34] employed nitrogen-doped graphene quantum dots (NGQDs) with gold on 3D-printed electrodes for DA detection. Their results indicated that the synergistic coupling between the highly conductive gold particles and nitrogen dopant sites significantly accelerated electron-transfer kinetics. However, this system was evaluated only in standard solutions and was not validated in biological matrices. Lima *et al.*[35] applied boron-functionalized N-doped graphene quantum dots for DA detection, relying on the electron-deficient boron atoms acting as Lewis's acid sites that promoted strong analyte adsorption, though this was only performed in buffer solutions without validation in real biological samples.

While these studies provide valuable insights into material design and electrochemical performance for DA detection, they do not address real-world clinical applicability and did not evaluate these materials in real human serum samples, particularly in clinical samples from epilepsy patients, highlighting an important gap that the present work addresses.

In contrast, the present study systematically evaluates the N-RGO platform in real human samples, including plasma from pediatric epilepsy patients. This approach enables not only sensitive detection of DA in complex biological matrices but also provides preliminary clinical insights into neurotransmitter dysregulation in epilepsy and the effects of drug such as VAL. To the best of our knowledge, this work represents the first preliminary clinical evaluation of electrochemical DA detection in pediatric epilepsy patients, bridging material innovation with translational application. Herein, we report the optimized synthesis of N-RGO and (S/N)-RGO nanomaterials and systematically evaluate their electrochemical behavior toward DA detection. The N-RGO platform was validated in commercial plasma, fresh human serum samples, and clinical samples from pediatric epilepsy patients, demonstrating its robustness and potential as a minimally invasive and reliable tool for real-time DA monitoring in clinical settings.

2 Materials and methods

2.1. Chemical reagents

RGO was synthesized and characterized using Fourier-transform infrared spectroscopy (FT-IR), X-ray photoelectron spectroscopy (XPS), cyclic voltammetry (CV), and electrochemical impedance spectroscopy (EIS), following a previously reported procedure.[36] GCEs and SPCEs were employed as working electrodes.

All chemicals and reagents, including dimethylformamide (DMF, 99.8%), ethanol (CH_3CH_2OH, 96%), acetone (CH_3COCH_3, ≥99.5%), phosphate-buffered saline (PBS, pH 7.4), dopamine hydrochloride (DA, 98%), L-ascorbic acid (AA, 99%), uric acid (UA, 99%), potassium chloride (KCl, 99.0–100.5%), ferricyanide/ferrocyanide ($[Fe(CN)_6]^{3-/4-}$), and ruthenium hexaamine ($[Ru(NH_3)_6]^{2+/3+}$), were purchased from Sigma-Aldrich (France).

PBS solutions were filtered through 0.22 μm syringe filters prior to use.

2.2. Biological materials

Human serum samples were obtained from healthy volunteers and pediatric epilepsy patients after signature of informed consent by patient parents as legal tutor, following local ethical regulations and institutional protocols (see section 2.8 Ethical issue following). No animal or/and animal's samples have been used in this study. Commercial plasma samples were purchased from Sigma-Aldrich (France). All solutions were prepared using deionized water from a Milli-Q purification system and freshly prepared daily to ensure reproducibility.

2.3. Synthesis of N-RGO

N-RGO was synthesized *via* a solvothermal method, as previously reported.[37] Typically, 600 mg of GO was dispersed in 60 mL of a Milli-Q water/ethanol mixture (1 : 1, v/v) by ultrasonication for 60 min. Then, 2 g of urea was added under vigorous magnetic stirring. The mixture was transferred into a 100 mL Teflon-lined autoclave and heated at 180 °C for 15 h. The resulting precipitate was centrifuged at 6500 rpm, washed repeatedly with water and ethanol, and dried in an oven at 80 ° C.

2.4. Synthesis of (S/N)-RGO

(S/N)-RGO was synthesized following the same procedure as N-RGO, replacing urea with thiourea as the dopant.

2.5. Preparation of modified GCEs

GCEs were sequentially polished with diamond pastes (6, 3, and 1 μm), ultrasonically cleaned in ethanol and acetone, rinsed with deionized water, and dried under nitrogen. A 10 μL aliquot of X-RGO suspension (X = N-RGO or (S/N)-RGO, 1 mg mL^{-1} in DMF) was drop-cast onto the GCE surface and dried in an oven at 80 °C for 45 min. The electrodes were then rinsed with ultrapure water to remove non-adsorbed material and residual DMF, and dried under nitrogen before use.

2.6. Preparation of modified SPCEs

SPCEs were first rinsed with deionized water to remove dust particles that could interfere with sensing. X-RGO (1 mg) was dispersed in DMF and sonicated for 1 h. Then, 2 μL of the resulting suspension was drop-cast onto the cleaned SPCE surface and dried in an oven at 45 °C overnight. SPCEs were selected for their disposability, ease of use, rapid response, reproducible electroactive surface area, and suitability for sensitive electrochemical detection.

2.7. Preparation of real samples

Blood serum samples were obtained from three healthy volunteers and four pediatric epilepsy patients, all of whom provided informed consent. Immediately after collection, blood samples were centrifuged at 3500 rpm for 5 minutes to ensure proper serum separation. The DA assay was performed immediately to avoid potential degradation caused by serological enzymes or storage conditions (congelation/de-congelation).

Before analysis, the resulting supernatants were diluted 10-fold with PBS (pH 7.4) to minimize matrix effects[38] and then spiked with known concentrations of DA using the standard addition method. No further pretreatment was applied.

For the commercial plasma samples, each sample was first dissolved in 5 mL of deionized water. A stock DA solution (1 μM) was then prepared in this plasma matrix, followed by serial dilutions to obtain the desired concentration range. The electrochemical response of the modified electrodes was evaluated using DPV.

2.8. Ethical issue

All procedures involving human serum samples were conducted in accordance with the ethical standards and of the institutional research committees and with the Declaration of Helsinki and its subsequent amendments. Ethical approval was obtained from the Ethics Committees of the Fatouma Bourguiba Hospital Monastir, Tunisia (approval no.: IOG 009738 no. 90/OMB 0990-0279), and the National Institute of Neurology, Tunisia (approval no.: 24/25). Written informed consent was obtained from all participants prior to inclusion in the study.

3 Results and discussion

In this work, electrochemical sensors based on RGO were developed, with heteroatom doping introduced to enhance electrocatalytic performance toward redox-active biomarkers. N-RGO and (S/N)-RGO were synthesized *via* a solvothermal approach, which effectively introduced electronic defects and increased the density of active sites. These features promoted stronger interactions with DA and accelerated electron transfer at the electrode interface. The electroactivity of the doped RGO (X-RGO) was found to depend on two main parameters: (i) the dispersibility of RGO in organic solvents, which enabled the formation of few-layered graphene nanosheets with a large surface area; and (ii) the improved charge transfer kinetics imparted by heteroatom incorporation. Structural and physicochemical characterizations confirming successful doping and morphological features are presented in the supplementary information (SI). The synthesized nanomaterials were employed as electrode modifiers for sensitive and selective DA detection. Analytical performance was first evaluated in PBS as a reference medium and further validated in real biological matrices, including commercial plasma and serum samples from pediatric epilepsy patients. This study represents the first preliminary electrochemical evaluation of DA levels in pediatric epilepsy patients, offering new insights into neurotransmitter dysregulation and highlighting the potential of heteroatom-doped RGO-based electrochemical platforms for clinical monitoring of neurological disorders.

3.1. Structural characterization

The synthesized X-RGO materials (X = N, (S/N)) were thoroughly characterized to confirm successful heteroatom doping and

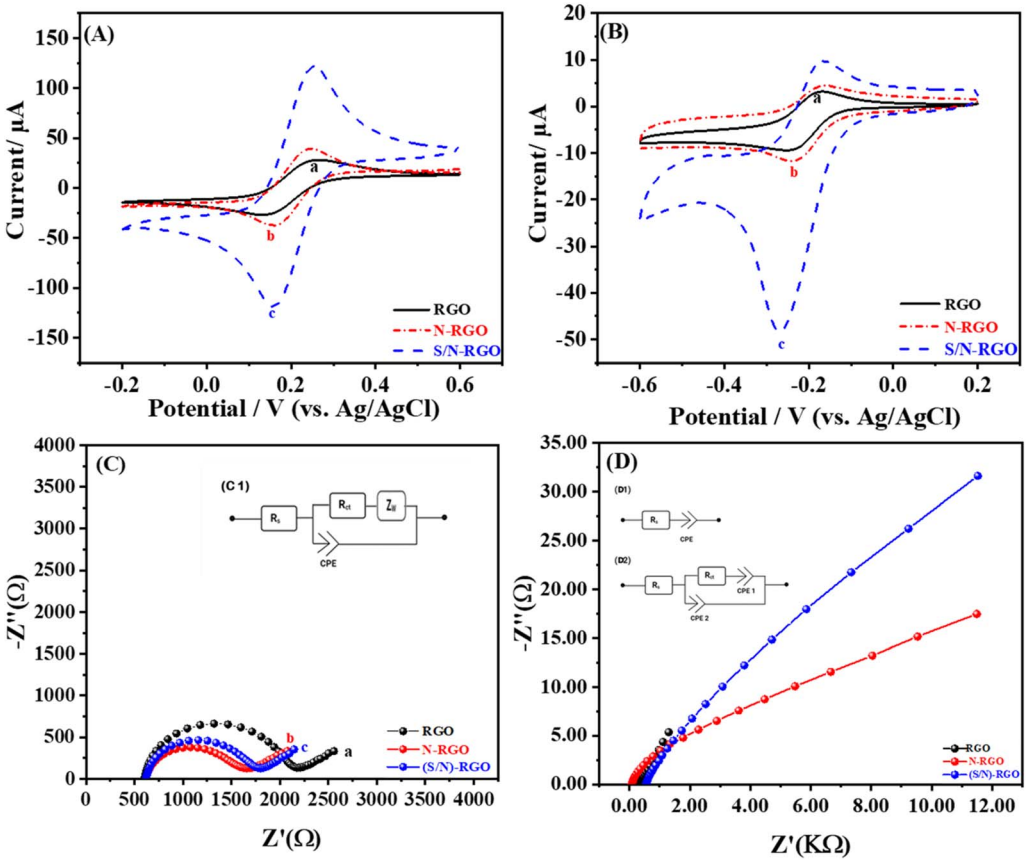

Fig. 1 CVs of (a) RGO/GCE, (b) N-RGO/GCE and (c) (S/N)-RGO/GCE recorded in (A) $[Fe(CN)_6]^{3-/4-}$ (10 mM, 0.1 M KCL) and (B) $[Ru(NH_3)_6]^{2+/3+}$ (10 mM, 0.1 M KCL) at scan rate of 50 mV s^{-1}. Nyquist plots of the different GCE electrodes from EIS measurements in the presence of (C) $[Fe(CN)_6]^{3-/4-}$ and $[Ru(NH_3)_6]^{2+/3+}$ (D). Insets show the equivalent circuit models used for fitting: (C1) Randles circuit consisting of solution resistance (R_s), charge transfer resistance (R_{CT}), constant phase element (CPE), and Warburg impedance (Z_w); (D1) simplified Randles circuit with a single CPE; (D2) extended model including two CPEs (CPE1 and CPE2), R_s, and R_{CT} accounting for interfacial processes on the electrode surface.

structural modification. Detailed analyses, including scanning electron microscopy (SEM), energy-dispersive X-ray spectroscopy (EDX), X-ray diffraction (XRD), FT-IR, and Raman spectroscopy, are provided in the supplementary information (SI). XPS measurements performed in a previous study also confirmed the presence of heteroatom-doping graphene.[24] These results confirm effective heteroatom incorporation and structural modification of RGO, which are expected to enhance electrochemical performance and facilitate strong interactions with target analytes.

3.2. Electrochemical characterization of doped RGO

To elucidate the mechanism of DA detection and assess the impact of heteroatom doping on electron transfer, the electrochemical performance of RGO, N-RGO, and (S/N)-RGO was investigated using CV, EIS, and scan-rate studies. Two distinct redox probes were employed: $[Ru(NH_3)_6]^{2+/3+}$, an outer-sphere redox system insensitive to surface chemistry that reflects the intrinsic conductivity of the electrode, and $[Fe(CN)_6]^{3-/4-}$, an inner-sphere redox system involving specific surface interactions that provides insights into interfacial electron transfer mechanisms.[39,40] These studies provide insights into how heteroatom doping influences the electron transfer kinetics, electroactive surface area, and DA detection efficiency.

CV measurements with $[Fe(CN)_6]^{3-/4-}$ (Fig. 1A, Table S3) revealed that N-RGO exhibited the lowest peak-to-peak separation (ΔE_p = 87 mV), compared to (S/N)-RGO (97 mV) and undoped RGO (119 mV), indicating faster electron-transfer kinetics. This enhancement is attributed to the incorporation of pyridinic and graphitic nitrogen species, which increase local electron density and the density of states (DOS), thereby facilitating redox reactions. In contrast, with $[Ru(NH_3)_6]^{2+/3+}$ (Fig. 1B, Table S4), ΔE_p values were 40 mV for N-RGO, 42 mV for RGO, and 43 mV for (S/N)-RGO, demonstrating that N-RGO also exhibits superior intrinsic electronic conductivity. Although the differences are modest, the consistently lower ΔE_p for N-RGO reflects a higher DOS and improved charge delocalization induced by nitrogen doping.

EIS measurements (Fig. 1C and D, Tables S5 and S6) further supported the CV findings. Nyquist plots indicated that the charge-transfer resistance (R_{CT}) decreased in the order RGO > (S/N)-RGO > N-RGO, with N-RGO showing the lowest R_{CT} values (996.8 Ω for $[Fe(CN)_6]^{3-/4-}$ and 40 kΩ for $[Ru(NH_3)_6]^{2+/3+}$). These

Table 1 Electrochemical parameters of RGO, N-RGO, and (S/N)-RGO electrodes obtained from CV and EIS measurements using $[Fe(CN)_6]^{3-/4-}$ and $[Ru(NH_3)_6]^{2+/3+}$ redox probes

Electrode	Redox probe	ΔE_p (mV)	R_{CT} (Ω)	Electroactive surface, A_{area} (cm^2)	Diffusion coefficient, D_0 ($cm^2\ s^{-1}$)	Heterogeneous rate constant, k_0 ($cm\ s^{-1}$)
RGO	$[Fe(CN)_6]^{3-/4-}$	119	1502.9	0.015	2.12×10^{-6}	2.32×10^{-3}
N-RGO	$[Fe(CN)_6]^{3-/4-}$	87	996.8	0.088	10.07×10^{-6}	7.49×10^{-3}
(S/N)-RGO	$[Fe(CN)_6]^{3-/4-}$	97	111.8	0.028	3.37×10^{-6}	5.71×10^{-3}
RGO	$[Ru(NH_3)_6]^{2+/3+}$	42	—	0.11	0.82×10^{-6}	0.07
N-RGO	$[Ru(NH_3)_6]^{2+/3+}$	40	40.8 K	0.44	3.94×10^{-6}	0.47
(S/N)-RGO	$[Ru(NH_3)_6]^{2+/3+}$	43	64.1 K	0.22	2.67×10^{-6}	0.28

results confirm the faster electron-transfer rate and superior electrochemical conductivity of N-RGO. In contrast, (S/N)-RGO showed slightly higher R_{CT} values, suggesting that sulfur incorporation may introduce minor lattice distortions, slightly hindering electron mobility and DA interactions. These results demonstrate that N-RGO significantly enhances both intrinsic charge transport and interfacial electron transfer, validating its effectiveness in modulating the graphene electronic network.

The electroactive surface area (A_{area}) was estimated from CV responses at various scan rates (50–500 mV s^{-1}) using the Randles–Sevcik equation (see Fig. S3, S4 and SI 1.3.1). A_{area} values varied depending on the redox probe due to differences in probe–electrode interactions: $[Fe(CN)_6]^{3-/4-}$ interacts strongly with surface functional groups, whereas $[Ru(NH_3)_6]^{2+/3+}$ predominantly reflects intrinsic conductivity. N-RGO exhibited the largest A_{area} for both probes (Table 1), confirming that nitrogen doping enhances layer exfoliation and the density of electroactive sites, thereby promoting DA adsorption and oxidation. The diffusion coefficients (D_0) for $[Fe(CN)_6]^{3-/4-}$ (7.6×10^{-6} $cm^2\ s^{-1}$) and $[Ru(NH_3)_6]^{2+/3+}$ (5.5×10^{-6} $cm^2\ s^{-1}$), along with the heterogeneous electron transfer rate constants (k_0), were determined using the Nicholson–Lavagnini formalism (see Fig. S5, S6 and SI 1.3.2) (ref de Nicholson et lavagnini). Both D_0 and k_0 were highest for N-RGO, highlighting a more favorable electronic environment for redox processes.

Overall, these results demonstrate that N-RGO is the optimal material for sensitive and selective DA detection, forming the basis for subsequent real-sample analyses, including preliminary clinical testing in pediatric epilepsy serum samples. Further electrochemical details, including diffusion coefficients and electron transfer rates, are provided in the supplementary information (SI, section 1.3).

3.3. Electrochemical comparison of modified electrodes for DA detection

DPV responses of the RGO, N-RGO, and (S/N)-RGO-modified SPCEs were conducted using 1 μM of DA in 0.1 M PBS (pH 7.4). The peak oxidation current increased markedly across the electrodes, with RGO/SPCE showing ~0.35 μA, N-RGO/SPCE exhibiting the highest current of 3.16 μA, and (S/N)-RGO/SPCE reaching 2.78 μA (Fig. 2). These results clearly demonstrate the influence of heteroatom doping on DA detection (Fig. 2). The pronounced enhancement observed for the N-RGO-modified electrode indicates faster electron transfer and stronger analyte–electrode interactions. This superior performance is attributed to nitrogen doping, which increases the density of electroactive sites and enhances electron-transfer efficiency, leading to higher peak currents for DA. RGO shows a lower peak current due to a reduced number of active sites, while (S/N)-RGO demonstrates slightly lower performance. This decrease may be due to sulfur incorporation, which can modify the graphene lattice, potentially introducing electronic effects constraints that partially hinder charge transfer due to the charge of sulfur and this behavior was demonstrated in previous study by DFT measurement showing that N/S doping led to the switch of electronic properties of graphene.[41] N-RGO demonstrates superior performance, making it ideal for sensitive DA detection in human plasma and further work will be performed will N-RGO.

3.4. Electrochemical detection of DA

The electrocatalytic activity of N-RGO and (S/N)-RGO-modified SPCEs toward DA oxidation was investigated in PBS (pH 7.4) within the potential window of 0.0–0.4 V (Fig. 3A and C).

Under optimized conditions, both modified electrodes exhibited a well-defined oxidation peak in DPV signal with peak

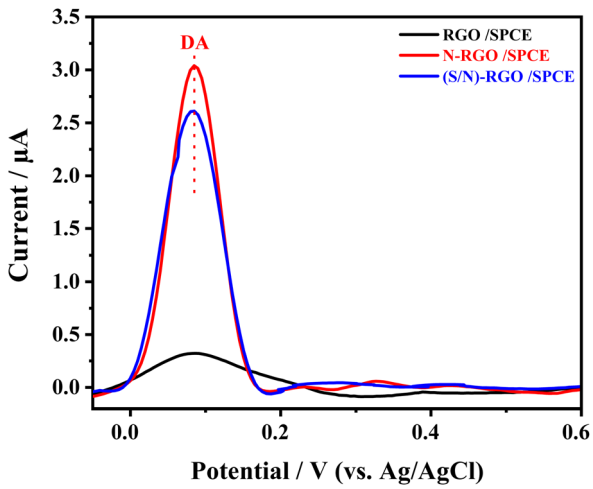

Fig. 2 DPV responses of the modified electrodes (RGO, N-RGO, (S/N)-RGO) toward DA were recorded in 0.1 M PBS (pH 7.4) containing 1 μM DA.

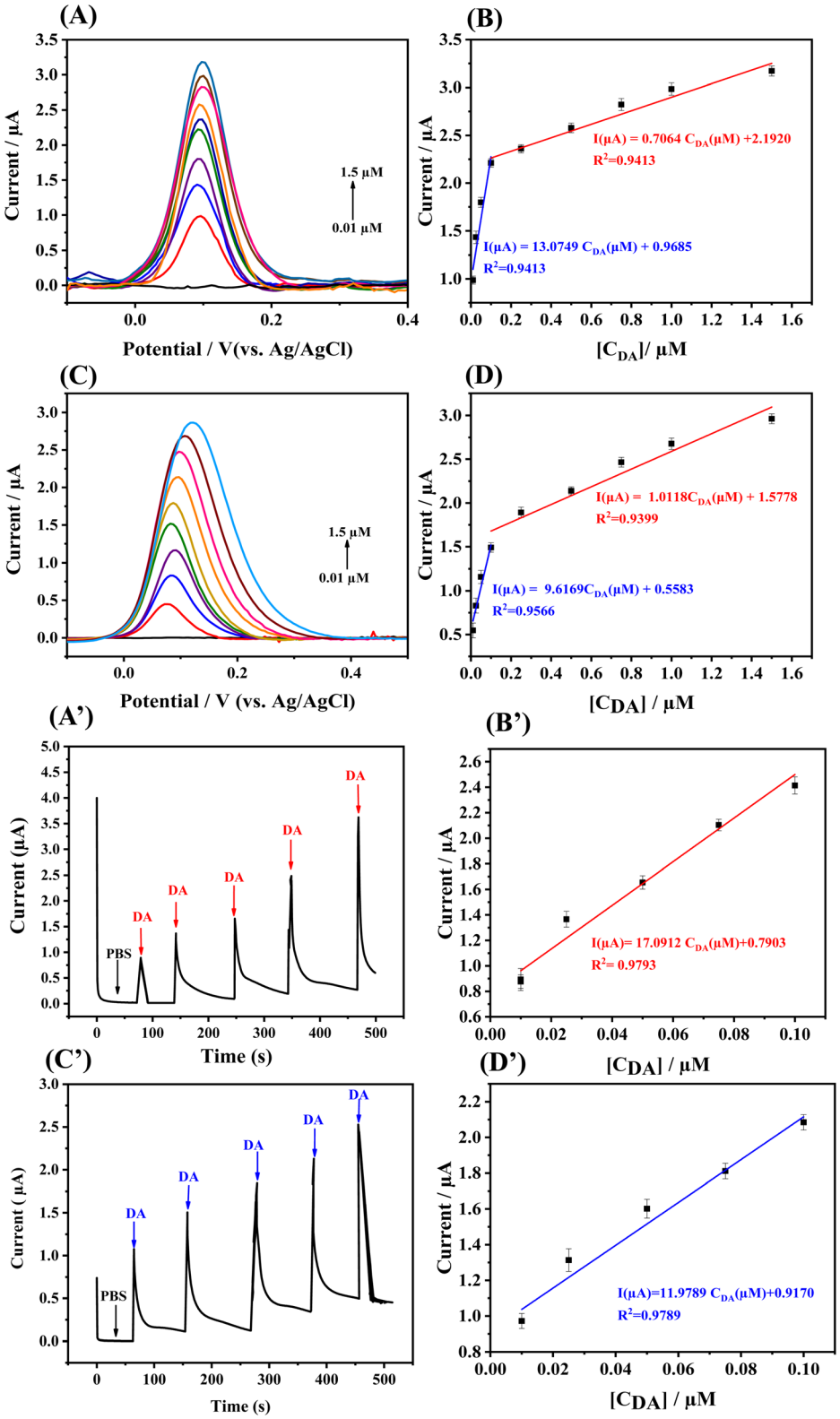

Fig. 3 DPV recorded for (A) N-RGO/SPCE and (B) (S/N)-RGO/SPCE in 0.1 M PBS (pH 7.4) containing increasing concentrations of DA: 0.01, 0.025, 0.05, 0.1, 0.25, 0.5, 0.75, 1.0, and 1.5 µM.Corresponding calibration plots of peak current *versus* DA concentration for N-RGO/SPCE (C) and (S/N)-RGO/SPCE (D). Amperometric responses of (A′) N-RGO/SPCE and (B′) (S/N)-RGO/SPCE upon successive additions of DA (0.01, 0.025, 0.05, 0.075, and 0.1 µM) at an applied potential of 200 mV in 0.1 M PBS. Corresponding calibration curves (C′ and D′).

Table 2 List of analytical performances of electrochemical sensors based on graphene for DA detection

Electrodes	Method	Applied potential (V)	Linear range (μM)	Limit of detection (LOD) (μM)	Ref.
GCE/N-rGO	DPV	—	0.5–170	0.25	45
GCE/N-rGO-180-8	DPV	—	2.5–100	0.63	46
GCE/N-rGO-180-8/NH3	DPV	—	0.5–150	0.41	46
CPE/N-rGO/CuCo2O	DPV	—	0.01–3	0.00331	47
3D graphene–CNT	Amperometric	+0.17	2.0–64.0	0.02	48
Graphene/Pt-modified GC	Amperometric	+0.30	0.03–8.13	0.03	49
GNC/CMG/GCE	Amperometric	+0.30	0.1–80	0.028	50
N-RGO/SPCE	Amperometric	+0.20	0.01–1	0.007	This study
N-RGO/SPCE	DPV	0.00–0.40	0.01–1.5	0.006	This study

currents increasing proportionally to DA concentration, confirming their effective catalytic behavior. A linear response was observed over the concentration range of 0.01–1.5 μM for both N-RGO/SPCE and (S/N)-RGO/SPCE (Fig. 3B and D) with two linear regressions depending of the range of the concentration. At low DA concentrations, the mechanism could be related to surface interaction behavior where the active sites of doped RGO surface favors the adsorption promoting higher current responses. Beyond a threshold concentration (~0.1 μM), a gradual saturation of these sites occurred, resulting in a diminished adsorption rate and a more gradual current increase where the diffusion process becomes a limiting step. The limits of detection (LOD) were calculated at a signal-to-noise ratio of 3, were 0.006 μM for N-RGO/SPCE and 0.018 μM for (S/N)-RGO/SPCE, with corresponding sensitivities of 13.079 μA μM^{-1} and 9.616 μA μM^{-1}, respectively.

Chronoamperometric measurements performed at 0.2 V (Fig. 3A′ and B′) further confirmed the rapid sensing capability of both modified electrodes. Upon successive additions of DA (0.01–0.1 μM), a stepwise increase in current was observed, with one linear calibration plots shown in Fig. 3C′ and D′. The resulting LODs were 0.007 μM for N-RGO/SPCE and 0.012 μM for (S/N)-RGO/SPCE, consistent with the DPV findings. These results clearly demonstrate the superior electrocatalytic efficiency of N-RGO/SPCE compared to (S/N)-RGO/SPCE.

This significant difference in performance can be explained by the underlying sensing mechanism. The sensing mechanism of DA on the modified electrodes involves adsorption and electron transfer at the defect sites introduced by heteroatom doping in the graphene structure. DA molecules interact with the graphene surface mainly through π–π stacking interactions between the aromatic ring of DA and the sp^2 carbon network, as well as hydrogen bonding and electrostatic interactions with surface functional groups. Nitrogen doping introduces electron-rich active sites (pyridinic, pyrrolic, and graphitic N) which enhance the local electronic density and promote faster electron transfer as it was also demonstrated in previous work.[42] These sites also strengthen the interaction with DA, resulting in an increased oxidation current and improved sensitivity. In contrast, in the case of (S/N)-RGO, sulfur co-doping alters the graphene lattice by introducing structural distortions due to the larger atomic radius of sulfur compared to carbon.[43] Although these defects may create additional adsorption sites, sulfur functionalities generally contribute less electron donation than nitrogen species, and can weaken the optimal planar configuration required for efficient π–π interactions with DA. Consequently, this structural and electronic perturbation results in lower sensitivity and a higher overpotential for DA oxidation on (S/N)-RGO compared with N-RGO.

The superior response of N-RGO is consistent with the findings of Wiench *et al.*,[44] who reported that pyrrolic and graphitic nitrogen functionalities increase electron density, promote faster charge transfer, and enhance π–π and electrostatic interactions with DA. These mechanisms explain the improved electrocatalytic behavior and lower LOD observed for N-RGO in this work.

Therefore, N-RGO emerges as a highly promising material for practical electrochemical sensing applications, particularly for the sensitive and selective DA detection in biological matrices. The obtained detection limits are lower than those reported of most graphene-based DA sensors, underscoring the outstanding analytical capabilities and practical potential of the proposed platform. A comparative summary of the analytical parameters is provided in Table 2.

3.5. Interference study and reproducibility

Selectivity is a critical parameter for DA detection in biological matrices, where common electroactive interferents such as AA and UA, typically coexist at higher physiological concentrations.[51] Selectivity studies were evaluated by DPV in the presence of these interferents, as shown in Fig. 4A.

Both N-RGO/SPCE and (S/N)-RGO/SPCE exhibited well-defined oxidation peaks for DA, AA, and UA. For N-RGO/SPCE, three well-separated oxidation peaks were observed at 54 mV, 190 mV, and 370 mV for AA, DA, and UA, respectively. The potential separations ($\Delta E_{(AA-DA)}$ = 136 mV) and ($\Delta E_{(DA-UA)}$ 180 mV) were sufficiently large to allow accurate discrimination of each species without cross-interference. Notably, N-RGO displayed the highest DA peak current even in presence of 10 times higher concentration of AA and UA, reflecting its superior electrocatalytic activity enhanced by their π–π and electrostatic interactions with DA.

In contrast, (S/N)-RGO exhibited the lowest DA oxidation current in the presence of interferents, with broader peaks and a slight shift in the oxidation potentials of DA, AA, and UA. This

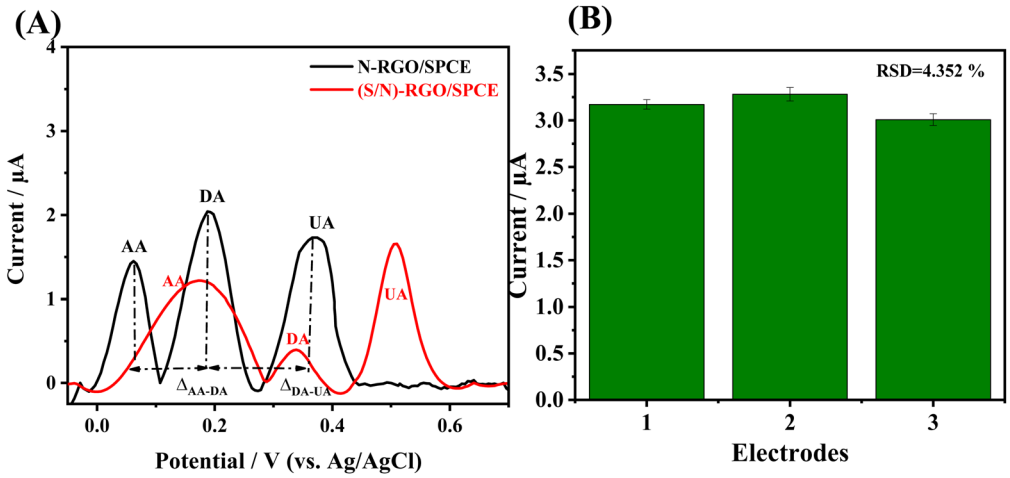

Fig. 4 DPVs of N-RGO/SPCE and (S/N)-RGO/SPCE electrodes recorded in supporting electrolyte 0.1 M PBS after adding 10 μM of UA, 10 μM of AA and 1 μM of DA (A). Results of reproducibility studies at three different electrodes in 1.5 μM DA (0.1 M PBS buffer, pH 7.4) (B).

discrepancy in DA behavior in the presence of others interferants, observed in both oxidation peak positions and currents between the N-RGO and (S/N)-RGO modified electrodes, can be attributed to the structural effects of heteroatom doping. Nitrogen doping alone introduces highly electron-rich active sites into the graphene lattice. These nitrogen species enhance the interaction between DA and the electrode surface, thereby facilitating electron transfer kinetics and enabling DA oxidation with higher current compared to the others interferents present at concentration 10 times higher. In contrast, sulfur co-doping in (S/N)-RGO introduces defects in the electronic structure and favors the interaction of other molecules, such AA and UA compared to DA due to their chemical structure enable electro-donating groups. Moreover, the slight positive shift of the DA oxidation potential in the ternary mixture relative to single-analyte measurements can be attributed to competitive adsorption at active sites and local interfacial effects, including proton generation from AA oxidation, which increases the overpotential required for DA oxidation. Same behavior was shown by Wei *et al.*,[52] whom reporting that the oxidation potentials of AA and DA shifted in multianalyte systems due to intermolecular interactions and concentration effects, highlighting the influence of coexisting electroactive species on peak positions.[52]

These observations confirm that, despite co-doping, (S/N)-RGO provides lower electrocatalytic activity and less favorable molecular recognition toward DA compared to N-RGO. Overall, the results highlight the superior selectivity of N-RGO/SPCE for reliable DA detection in complex biological matrices.

To evaluate the reproducibility of the developed sensor, three independent N-RGO-modified SPCEs were fabricated under identical conditions by drop-casting 2 μL of the N-RGO dispersion onto the electrode surface. The electrochemical response toward 1.5 μM DA was recorded for each electrode. As presented in Fig. 4B, the three electrodes exhibited nearly identical current responses, with a relative standard deviation (RSD) of 4.35%, demonstrating good reproducibility. This low deviation confirms the reliability and stability of the N-RGO/SPCE sensor for consistent detection of DA. Minor variations can be attributed to small differences in the intrinsic conductivity of individual SPCE substrates or slight non-uniformities in the thickness of the N-RGO film during drop-casting.[53]

3.6. Determination of DA in commercial plasma samples

To assess the practical applicability of the N-RGO/SPCE sensor in complex biological matrices, DA detection was first carried out in commercial plasma samples. DPV was employed due to its high sensitivity and its ability to discriminate overlapping electrochemical signals. Prior to analysis, plasma samples were diluted with buffer solution to reduce matrix viscosity and mitigate protein content, which can attenuate electrochemical responses.

The standard addition method was adopted to minimize matrix effects, by spiking the diluted plasma with known concentrations of DA. The DPV response of the un-spiked plasma showed no detectable oxidation peak within the potential window, confirming the absence of interfering endogenous electroactive species. Upon the addition of DA, distinct anodic peaks were observed and increased proportionally with DA concentration (Fig. 5A), demonstrating the sensor's capability for quantitative analysis in a plasma.

The calculated recovery rates ranged from 113.6% to 116.0%, with low RSDs of 1.99% and 1.87% ($n = 3$), indicating high accuracy and reproducibility. The slightly higher recovery values likely result from weak DA–protein interactions in plasma, leading to local preconcentration and enhanced oxidation signals.

These findings confirm the robustness of the N-RGO/SPCE platform in maintaining sensitivity and selectivity, even in the presence of complex biological components, highlighting its strong potential for clinical diagnostics involving blood-derived samples. Detailed analytical results are summarized in Table 3.

3.7. Preliminary evaluation of the electrochemical DA sensor in the clinical field

The feasibility of the developed sensor for real biomedical applications was further assessed using freshly collected

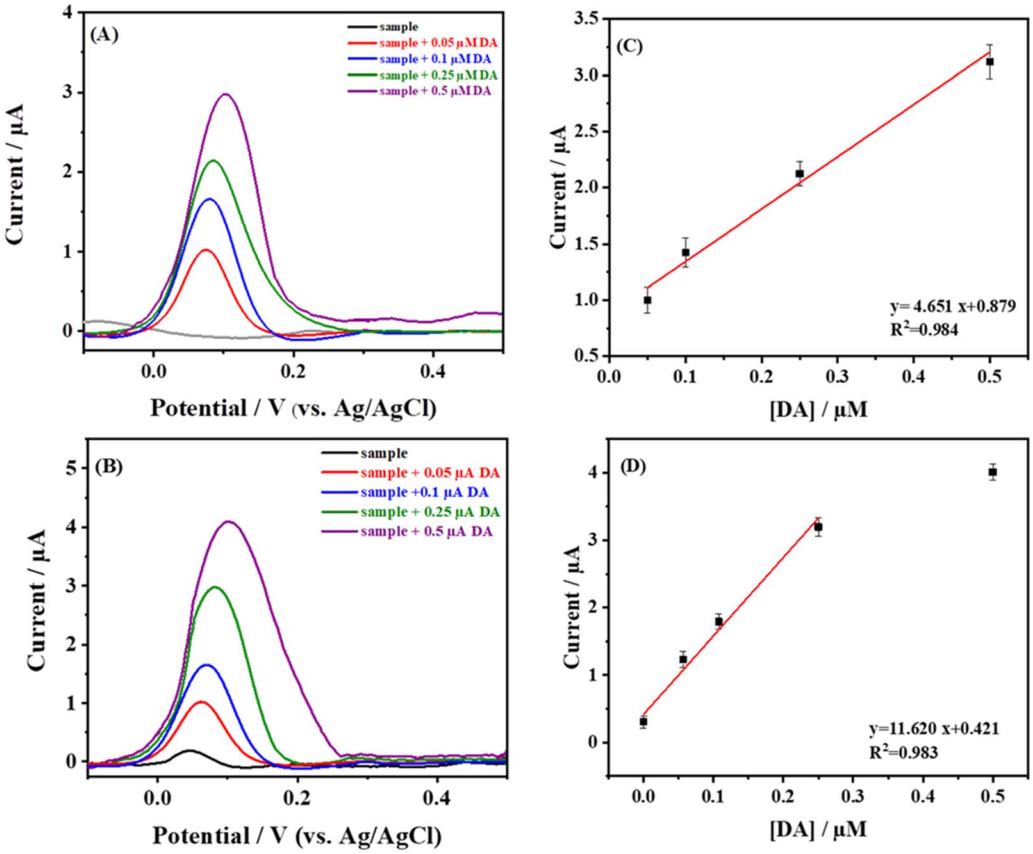

Fig. 5 DPV recorded at a scan rate of 50 mV s^{-1} from the measurement of 0.1 M phosphate buffer (pH 7.4) solution containing: (A) commercial plasma sample, (B) human blood serum spiked with various concentrations of DA using SPCE/N-RGO. (C and D) Calibration plot of the concentration of DA.

Table 3 Determination of DA in healthy human serum and plasma samples using DPV

Sample type	DA added (μM)	DA found (μM)	Recovery (%)	RSD (%) ($n = 3$)
Commercial plasma	0.05	0.056	112.0	1.99
	0.25	0.284	113.6	1.87
Healthy human serum	0.00	0.030	—	3.18
	0.05	0.081	101.1	1.18
	0.25	0.294	105.0	1.75

human serum samples from healthy donors. Under physiological conditions, DA concentrations in serum typically range between 0.03 μM and 0.2 μM;[8,9] therefore, accurate detection within this range is essential for early diagnosis and therapeutic monitoring of neurological disorders. To reduce viscosity and remove interfering macromolecules, serum samples were diluted 10-folds with PBS (pH 7.4) and prior to measurement to prevent electrode fouling and maintain reproducible response.

DPV measurements of diluted serum revealed an endogenous DA concentration of 0.03 μM (Fig. 5B). This result aligns well with the physiological DA levels reported in healthy individuals, confirming the analytical reliability of the N-RGO/SPCE sensor. Recovery rates ranged from 101.1% to 105.0%, with RSDs between 1.18% and 3.18%, further demonstrating excellent precision and sensor robustness in complex biological fluids (see SI 1.4).

The results summarized in Table 3 validate the sensor's ability to accurately quantify DA in real serum samples within clinically relevant ranges. These findings highlight the strong potential of the N-RGO/SPCE device for practical DA assays and support its future integration into POC diagnostics and continuous monitoring tools for DA-related neurological disorders.

Following these results, it is hypothesized that DA levels in epileptic patients may fluctuate according to seizure phase and antiepileptic drug (AED) treatment. Typically, DA concentrations are expected to be low during interictal (non-seizure) periods, elevated during seizure episodes, and moderately

Table 4 DA concentrations measured in serum samples of pediatric patients using N-RGO/SPCE

Patients	Clinical status	VAL treatment	DA level (nM)
Child1 (10 years)	Control	No	1.2
Child 2 (13 years)	EAE	Yes (4 years)	19.0
Child 3 (8 years)	Control	No	10.4
Child 4 (7 years)	Focal epilepsy with cavernomas, VAL-resistant	Yes (long term)	150.0

regulated under chronic AED therapy with VAL.[54] DA serves as a key neuromodulator regulating the excitatory-inhibitory balance in the central nervous system through interactions with glutamatergic and GABAergic pathways. During epileptic activity, excessive glutamate release induces neuronal hyperexcitability, while insufficient GABAergic inhibition fails to restore homeostasis. In response, the dopaminergic system is activated as a compensatory mechanism to enhance GABAergic activity and mitigate glutamate-induced excitotoxicity.[55]

The interaction between AEDs and the dopaminergic system is of particular neurophysiological relevance. Medications such as phenobarbital and VAL are known to modulate DA release, influencing dopaminergic tone both centrally and peripherally. These alterations may contribute not only to seizure control but also to the emergence of neuropsychiatric and neuromuscular side effects, including altered mood, motivation, or motor control. Monitoring DA levels in patients under chronic AED therapy may therefore provide valuable insights into treatment efficacy and drug-related neurochemical effects. In the present study, the N-RGO/SPCE sensor was employed for quantification of serum DA levels in four pediatric subjects representing two different clinical epilepsy presentations, along with two controls (Table 4) (see SI, Fig. S8 and S7).

The first clinical presentation involved Child 1 and Child 2. Child 1, diagnosed with epilepsy but untreated, exhibited a markedly low serum DA level (1.2 nM), consistent with hypodopaminergic activity. In contrast, Child 2, diagnosed with epilepsy with absence seizures (EAE) and treated with VAL for four years, a condition typically characterized by hypodopaminergic deficiency,[5] showed a normalized DA concentration of approximately 0.019 μM, suggesting that long-term VAL therapy may stabilize dopaminergic neurotransmission and restore physiological balance.

The second clinical presentation included Child 3 and Child 4. Child 3, a healthy control, displayed DA levels within the normal physiological range (0.01 μM). Child 4, diagnosed with pharmaco-resistant paroxysmal focal epilepsy (EpfPh) associated with multiple cavernomas, exhibited a significantly elevated DA concentration. This observation is consistent with reports indicating that chronic VAL exposure can enhance peripheral DA release, leading to elevated serum concentrations in that case.[56] Moreover, Child 4 showed major fluctuations in VAL serum levels over several years of treatment (initiated at 6 months of age), supporting the hypothesis that irregular DA levels may correlate with treatment resistance and impaired dopaminergic regulation.

These results demonstrate the distinct impact of VAL antiepileptic treatment on dopaminergic modulation across different epileptic syndromes. The contrasting profiles of Child 2 (generalized epilepsy) and Child 4 (focal epilepsy) highlight the complexity of epilepsy physiopathology and reveal the heterologous influence of AEDs on dopamine regulation. These findings clearly underline the added value of using the N-RGO/SPCE sensor for the DA assay. This platform may help clinicians better understand the complex physiopathology of epileptic seizures and their interaction with VAL treatment in real time and to modulate the treatment in function of such modification in the physiopathology of the disease during long term evolution.

The developed noninvasive DA detection system has proven its efficiency for detecting nanomolar concentrations of DA in simple biological matrix without need of pretreatment. These findings confirm the sensor's potential as a powerful diagnostic and monitoring tool for epilepsy monitoring and treatment modulation effect, then its use could broadly be enlarged for neurological and psychiatric disorders associated with dopaminergic dysregulation.

4 Conclusions

In this study, a disposable electrochemical sensor was developed for the highly sensitive detection of DA in simple and noninvasive biological fluid (blood serum), using heteroatom-doped RGO as the electrode modifier. The N-RGO/SPCE sensor demonstrated remarkable sensitivity and selectivity, attributed to the synergistic effects of nitrogen functionalities, which facilitate electron transfer and strengthen π–π interactions with the DA. As result, the sensor achieved a low LOD of 6.8 nM and a broad linear detection range of 0.01–1.5 μM. In addition, it exhibited excellent analytical reliability, with recovery rates exceeding 100% and RSD values below 3%, even in complex biological matrices.

Beyond analytical validation, the N-RGO/SPCE platform was applied in clinical context for monitoring DA levels in pediatric epilepsy undergoing VAL therapy. This application revealed DA fluctuations correlated with treatment status, highlighting not only the robustness of the sensing platform but also its potential as a valuable analytical tool for neurochemical diagnostics, and therapeutic monitoring. The combination of high analytical performance, disposability, and ease of fabrication demonstrates that the N-RGO/SPCE sensor is a promising system for the development of POC devices aimed at real-time monitoring of NTs in clinical settings.

Ethics approval and consent to participate

The use of human serum samples for research was approved by the ethics committee affiliated with the University Hospital of Monastir, Tunisia (ethical approval number: IOG 009738 no. 90/OMB 0990-0279). The collection of blood serum samples from paediatric epileptic patients undergoing treatment with valproic acid (VPA) was approved by the ethics committee of the National Institute of Neurology in Tunis (ethical approval number: 24/25).

Conflicts of interest

The authors report no financial disclosures or competing interests relevant to this study.

Data availability

The data supporting this article have been included as part of the supplementary information (SI) at "Sciences Data Bank". See DOI: Said Galai. Supplementary informations data [DS/OL]. V1. Science Data Bank, 2025 [2025-12-18]. https://doi.org/10.57760/sciencedb.33895. Data of patient code cited in this article cannot be made available, for ethical confidentiality requirements. Supplementary information: the structural and morphological characters of the modified electrode, the method used for determination of DA in real sample and the ethical document used for this work. See DOI: https://doi.org/10.1039/d5ra09797e.

Acknowledgements

This research was funded by PHC Maghreb 20MAG22 and International Emerging Action CNRS (France-Tunisia) project. Authors thanks the fund provided from ministry of Europe and Foreign affairs of France and ministry of Higher Education and Scientific Research of Tunisia, for the fund of PHC Maghreb 20MAG22. Authors also thanks CNRS for co-funding IEA (France-Tunisia) project.

References

1 C. Labandeira, A. Fraga-Bau, D. Arias Ron, E. Alvarez-Rodriguez, P. Vicente-Alba, J. Lago-Garma and A. Rodriguez-Perez, *Neural Regen. Res.*, 2022, **17**, 1652.
2 J. Huang, *et al.*, *Front. Aging Neurosci.*, 2020, **12**, 574023.
3 C. Huang, S. Pan, W. Chin, Y. Chen, C. Wu, C. Hsu, P. Lin, P. Chen and Y. L. Guo, *Environ. Res.*, 2022, **212**, 113128.
4 T.-S. Chen, T.-H. Huang, M.-C. Lai and C.-W. Huang, *Biomedicines*, 2023, **11**, 783.
5 F. Cavarec, P. Krauss, T. Witkowski, A. Broisat, C. Ghezzi, S. De Gois, B. Giros, A. Depaulis and C. Deransart, *Epilepsia*, 2019, **60**, 2128–2140.
6 M. O. Klein, D. S. Battagello, A. R. Cardoso, D. N. Hauser, J. C. Bittencourt and R. G. Correa, *Cell. Mol. Neurobiol.*, 2019, **39**, 31–59.
7 D. S. Goldstein, K. J. Swoboda, J. M. Miles, S. W. Coppack, A. Aneman, C. Holmes, I. Lamensdorf and G. Eisenhofer, *J. Clin. Endocrinol. Metab.*, 1999, **84**, 2523–2531.
8 G. Eisenhofer, I. J. Kopin and D. S. Goldstein, *Pharmacol. Rev.*, 2004, **56**, 331–349.
9 O. Hornykiewicz, in *Parkinson's Disease and Related Disorders*, eds. P. Riederer, H. Reichmann, M. B. H. Youdim and M. Gerlach, Springer Vienna, Vienna, 2006, pp. 9–15.
10 P. R. Reid, W. L. Thompson, *et al.*, *Johns Hopkins Med. J.*, 1976, **20**(139), 506.
11 V. Carrera, *et al.*, *J. Chromatogr. B*, 2007, **847**, 88–94.
12 J. F. Van Staden and R. I. S. Van Staden, *Talanta*, 2012, **102**, 34–43.
13 C. Zhao, Y. Jiao, J. Hua, J. Yang and Y. Yang, *J. Fluoresc.*, 2018, **28**, 269–276.
14 X. Li, J. Pan, F. Yang, J. Feng, J. Mo and Z. Chen, *Microchim. Acta*, 2011, **174**, 123–130.
15 W. Liu, F. Cui, H. Li, S. Wang, B. Zhuo and S. Wang, *Sens. Actuators, B*, 2020, **323**, 128669.
16 H. M. Alsoghier, *et al.*, *Sci. Rep.*, 2024, **14**, 16601.
17 A. Cirocka, D. Zarzeczańska and A. Wcisło, *Materials*, 2021, **14**, 4743.
18 R. D. Crapnell and C. E. Banks, *ChemElectroChem*, 2024, **11**, e202400370.
19 R. M. Silva, A. D. Da Silva, J. R. Camargo, B. S. De Castro, L. M. Meireles, P. S. Silva, B. C. Janegitz and T. A. Silva, *Biosensors*, 2023, **13**, 453.
20 S. Palanisamy, B. Thirumalraj, S. Chen, M. Ajmal Ali, K. Muthupandi, R. Emmanuel, P. Prakash and F. M. A. Al-Hemaid, *Electroanalysis*, 2015, **27**, 1998–2006.
21 Z. Hsine, R. Mlika, N. Jaffrezic-Renault and H. Korri-Youssoufi, *Chemosensors*, 2022, **10**, 249.
22 S. K. Tiwari, S. Sahoo, N. Wang and A. Huczko, *J. Sci.: Adv. Mater. Devices*, 2020, **5**, 10–29.
23 M. Pumera, *J. Mater. Chem. C*, 2014, **2**, 6454–6461.
24 F. Besbes, Z. Hsine and R. Mlika, *Carbon Lett.*, 2023, **33**, 2109–2128.
25 S.-Y. Hsu, C.-L. Lee, C.-H. Kuo and W.-C. Kuo, *Sens. Actuators, B*, 2021, **328**, 129015.
26 T. Jiang, H. Zhai, K. Yang, Z. Tang, T. Chen, Y. Liu, X. Liu, Y. Xue and M. Wu, *Int. J. Electrochem. Sci.*, 2024, **19**, 100434.
27 Z.-H. Sheng, L. Shao, J.-J. Chen, W.-J. Bao, F.-B. Wang and X.-H. Xia, *ACS Nano*, 2011, **5**, 4350–4358.
28 N. H. A. Rosli, *et al.*, *Diamond Relat. Mater.*, 2021, **120**, 108696.
29 K. Parvez, R. A. Rincón, N.-E. Weber, K. C. Cha and S. S. Venkataraman, *Chem. Commun.*, 2016, **52**, 5714–5717.
30 S. Kumar, S. Patra, R. Madhuri and P. K. Sharma, in *DAE Solid State Physics Symposium*, 2016, 2017050068.
31 W. Zhu, J. Gao, H. Song, X. Lin and S. Zhang, *ACS Appl. Mater. Interfaces*, 2019, **11**, 44545–44555.
32 L. Xiao, J. Yin, Y. Li, Q. Yuan, H. Shen, G. Hu and W. Gan, *Analyst*, 2016, **141**, 5555–5562.

33 H. Zhang and S. Liu, *J. Alloys Compd.*, 2020, **842**, 155873.
34 L. Zhong, X. Du, Y. Jiang, J. Wen, X. Wang, W. Shuoti, R. Peng, M. Liao, J. Ou, Y. Yang and L. Wang, *Microchem. J.*, 2025, **212**, 113432.
35 A. R. S. Lima, A. Mikhraliieva, C. R. Vanoni, M. Nazarkovsky, Y. Xing, M. T. Couto, V. Zaitsev and C. L. Jost, *Diamond Relat. Mater.*, 2024, **146**, 111259.
36 E. Kusrini, A. A. Suhrowati, A. Usman, V. Degirmenci Dr and M. Khalil, *Int. J. Technol. Manag.*, 2019, **10**, 1093.
37 M. H. Elbakkay, W. M. A. El Rouby, S. I. El-Dek and A. A. Farghali, *Appl. Surf. Sci.*, 2018, **439**, 1088–1102.
38 Z. Hsine, S. Blili, R. Milka, H. Dorizon, A. H. Said and H. Korri-Youssoufi, *Anal. Bioanal. Chem.*, 2020, **412**, 4433–4446.
39 R. L. McCreery, *Chem. Rev.*, 2008, **108**, 2646–2687.
40 N. S. Komarova, A. G. Krivenko, E. V Stenina and L. N. Sviridova, *J. Electroanal. Chem.*, 2017, **788**, 1–6.
41 J. H. Lee, *et al.*, *Nanomaterials*, 2019, **9**, 268.
42 H. Moradpour and H. Beitollahi, *C*, 2022, **8**, 50.
43 F. Liu, J. Niu, X. Chuan and Y. Zhao, *J. Alloys Compd.*, 2023, **947**, 169654.
44 P. Wiench, Z. González, S. Gryglewicz, R. Menéndez and G. Gryglewicz, *J. Electroanal. Chem.*, 2019, **852**, 113547.
45 X. Feng, Y. Zhang, J. Zhou, Y. Li, S. Chen, L. Zhang, Y. Ma, L. Wang and X. Yan, *Nanoscale*, 2015, **7**, 2427–2432.
46 P. Wiench, Z. González, R. Menéndez, B. Grzyb and G. Gryglewicz, *Sens. Actuators, B*, 2018, **257**, 143–153.
47 F. Tadayon and Z. Sepehri, *RSC Adv.*, 2015, **5**, 65560–65568.
48 X. Dong, *et al.*, *J. Mater. Chem.*, 2012, **22**, 17044.
49 C.-L. Sun, H.-H. Lee, J.-M. Yang and C.-C. Wu, *Biosens. Bioelectron.*, 2011, **26**, 3450–3455.
50 S. Daemi, A. A. Ashkarran, A. Bahari and S. Ghasemi, *J. Colloid Interface Sci.*, 2017, **494**, 290–299.
51 Y. Vadivelu, A. Sendrayal Raj, R. Muniyandi, S. R. Srither and B. Ramachandran, *Talanta Open*, 2025, **12**, 100477.
52 Y. Wei, Y. Liu, Z. Xu, S. Wang, B. Chen, D. Zhang and Y. Fang, *Int. J. Anal. Chem.*, 2020, **2020**, 1–13.
53 A. Dube, S. J. Malode, A. N. Alodhayb, K. Mondal and N. P. Shetti, *Talanta Open*, 2025, **11**, 100395.
54 R. H. Mattson, J. A. Cramer, P. D. Williamson and R. A. Novelly, *Ann. Neurol.*, 1978, **3**, 20–25.
55 B. Calvo-Flores Guzmán, C. Vinnakota, K. Govindpani, H. J. Waldvogel, R. L. M. Faull and A. Kwakowsky, *J. Neurochem.*, 2018, **146**, 649–669.
56 Y. Bozzi and E. Borrelli, *Front. Cell. Neurosci.*, 2013, **7**, DOI: 10.3389/fncel.2013.00157.